Evidence for one-pion charge exchange in $^{13}N + {}^{13}C$ elastic scattering near the Coulomb barrier

E. Liénard,[1,*] D. Baye,[2] Th. Delbar,[1] P. Descouvemont,[2] P. Duhamel,[3] W. Galster,[1] M. Kurokawa,[4,†] P. Leleux,[1] I. Licot,[1] P. Lipnik,[1] C. Michotte,[1] T. Motobayashi,[4] A. Ninane,[1] J.-M. Sparenberg,[2] J. Vanhorenbeeck,[3] and J. Vervier[1]

[1] *Institut de Physique Nucléaire, Université Catholique de Louvain, B 1348 Louvain-la-Neuve, Belgium*

[2] *Physique Nucléaire Théorique et Physique Mathématique, Code Postal 229, Université Libre de Bruxelles, B 1050 Brussels, Belgium*

[3] *Institut d'Astronomie et d'Astrophysique, Code Postal 226, Université Libre de Bruxelles, B 1050 Brussels, Belgium*

[4] *Department of Physics, Rikkyo University, Toshima, Tokyo 171, Japan*

(Received 8 July 1996)

Elastic $^{13}N + {}^{13}C$ cross sections are measured at center-of-mass energies of 8.15, 10.0, and 14.75 MeV, using a radioactive ^{13}N beam and position-sensitive solid-state detectors. The $^{13}N + {}^{13}C$ angular distributions display oscillations beyond 80° and even a significant rise at large angles for the two higher energies. These data are analyzed in the framework of the optical model including a parity-dependent term necessary to explain the backward behavior. This parity term is among the strongest encountered in heavy-ion collisions. Its properties are close to those of the parity term reproducing the $^{13}N + {}^{12}C$ elastic scattering in the same energy range. Its long-range nature indicates that the parity dependence arises from a single rather than from a double exchange. One-pion charge exchange between the valence nucleons seems to possess the necessary properties as qualitatively shown by a simple molecular model. [S0556-2813(96)05311-3]

PACS number(s): 25.60.Bx, 24.10.Ht, 25.60.Lg, 25.70.Kk

I. INTRODUCTION

The existence of radioactive ion beams allows for the first time a detailed exploration of the isospin degrees of freedom in nuclear reactions [1]. Replacing in a collision a nucleus by another nucleus with the same mass number becomes possible [2,3]. Such studies were until now severely limited by the fact that pairs of stable isobars do not exist for mass numbers smaller than 36. They were restricted to cases where long-lived isotopes such as ^{3}H, ^{7}Be, or ^{14}C are available.

Recently charge symmetry could be studied in a comparative study of the mirror $^{13}N + {}^{12}C$ and $^{13}C + {}^{12}C$ elastic collisions [2,3]. The elastic cross sections at three energies in the vicinity of the Coulomb barrier were analyzed with the optical model assuming the same real central part of the nuclear potential for both systems as suggested by charge symmetry. The absorptions which depend on threshold energies and elastic-transfer effects which depend on the tails of the individual wave functions of the valence nucleon are both sensitive to the Coulomb interaction. Therefore they are different in mirror collisions. Differences in the parity terms simulating the elastic transfer of the valence nucleon are well understood. Differences of absorption seem to be mostly due to the coupling with direct channels, and especially with inelastic channels. Except for these known differences, charge symmetry applies as a good approximation to the central part of the nucleus-nucleus interaction.

Collisions between distinct mirror nuclei provide an even more interesting challenge because they are not realizable without radioactive nuclei, so that their properties remain essentially unknown at present. Here we report on a first experimental study of the $^{13}N + {}^{13}C$ elastic scattering at energies close to the Coulomb barrier (preliminary accounts can be found in Refs. [4,3]). In marked contrast with the pair of mirror $^{13}N + {}^{12}C$ and $^{13}C + {}^{12}C$ elastic collisions which are strongly related to each other, the $^{13}N + {}^{13}C$ collision is essentially distinct from $^{13}C + {}^{13}C$ because of different isospin contents: While $^{13}C + {}^{13}C$ is purely $T=1$, $^{13}N + {}^{13}C$ contains a mixing of $T=0$ and $T=1$ components. Moreover, while the $^{13}C + {}^{13}C$ cross sections are symmetric with respect to 90°, $^{13}N + {}^{13}C$ provides useful information up to large angles. It offers a better opportunity of probing the interaction between these nuclei.

The postaccelerated ^{13}N radioactive beam at the Louvain-la-Neuve facility allows us to study the $^{13}N + {}^{13}C$ collision with intensities of about 1.2×10^{8} particles per second. Experiments were carried out at three laboratory energies 16.3, 20.0, and 29.5 MeV with an energy resolution of about 0.3 to 0.6 MeV. In the center-of-mass (c.m.) frame, these energies correspond to 8.15, 10.0, and 14.75 MeV, respectively, covering an energy range from just above to about twice the Coulomb barrier. This collision involves two different nuclei with identical ^{12}C cores but different valence nucleons. Therefore the elastic cross sections simultaneously contain contributions from core exchange and from charge exchange between the valence nucleons. Its analysis brings physical information which is not available from other collisions. Only the $^{3}He + {}^{3}H$ [5] and $^{7}Be + {}^{7}Li$ [6] collisions were until now accessible for such studies. The former is, however, restricted to a small number of partial waves and the latter is rendered complicated by the high spins and deformations of the colliding nuclei. At low energies, the $^{13}N + {}^{13}C$ scattering at backward angles is expected to be sensitive

*Present address: GANIL, 14021 Caen, France.

†Present address: RIKEN, Hirosawa, Wako, Saitama 351-01, Japan.

to exchange effects such as elastic nucleon transfers or charge exchange.

The $^{13}N + {}^{13}C$ collision has been analyzed schematically in the framework of a molecular orbital model in Ref. [7]. The same model was later applied in a numerical prediction of the $^{13}N + {}^{13}C$ cross sections at energies below 10 MeV [8]. The results exhibit no significant backward rise. The authors of Ref. [8], being aware of very preliminary results of the present experiment, conjecture that pion exchange effects might significantly modify the behavior at large angles.

Let us mention that another experimental study of the $^{13}N + {}^{13}C$ collision has been recently performed in a very different energy range, i.e., at $E/A=57$ and 105 MeV with respective intensities of 5×10^6 and 6×10^5 particles per second and with energy resolutions around 1 MeV [9]. The authors of Ref. [9] attempt to measure Gamow-Teller transition strengths with heavy ion collisions. They focus on charge transfer at 0°.

The experimental setup and the results are described in Sec. II. An optical-model study of these data is performed in Sec. III. The interpretation of the resulting potential is discussed in Sec. IV. Concluding remarks are presented in Sec. V.

II. EXPERIMENTAL PROCEDURE

The experimental setup is described thoroughly in a previous paper [2]. In brief, $^{13}N^{2+}$ beams [10] of 16.3, 20.0, and 29.5 MeV energies and of 1.2×10^8 pps typical intensity bombard a self-supporting ^{13}C target of 40 μg/cm^2 thickness. Two large ion-implanted silicon detectors record the scattered ^{13}N and the recoiling ^{13}C ions; each detector is made of 12 resistive horizontal strips, 60 mm long × 5 mm wide, with a passive gap of 50 μm between successive strips. They are located at mean distances of 20 and 25 cm from the target, covering angular ranges of 13° and 15° in the laboratory system, respectively. With this setup, the angular distributions of the $^{13}N + {}^{13}C$ elastic scattering are obtained from 15° to 150° in the c.m. frame with only two angle settings. At each energy, some data are also recorded with a stable ^{13}C beam [2]. Apart from checking the consistency with existing data [11], they are useful at several levels, as it will appear later. Signals from both ends of each strip yield the energy and the position of the particles. The energy and position calibration of the detectors are obtained from the ^{13}C + Au scattering and from the transmission of α particles from an ^{241}Am source, through a grid with seven vertical slits placed in front of the detectors. Conventional electronics and a CAMAC-VME data acquisition system are used to analyze the data.

The detectors are located at forward angles in the laboratory and they record scattered ^{13}N ions (forward c.m. angles) and recoiling ^{13}C ions (backward c.m. angles). To increase the energy difference between both species, a 1 mg/cm^2 thick Al foil is placed in front of the detectors, inducing a typical energy loss difference of 1 MeV between ^{13}C and ^{13}N. The full width at half maximum (FWHM) of the ^{13}N and ^{13}C peaks is of the order of 600 keV, resulting from the convolution of several factors: the energy width of the cyclotron beam ($\Delta E/E\approx2\%$ FWHM), the angular resolution, arising from the 4 mm diameter beam spot on target (1°),

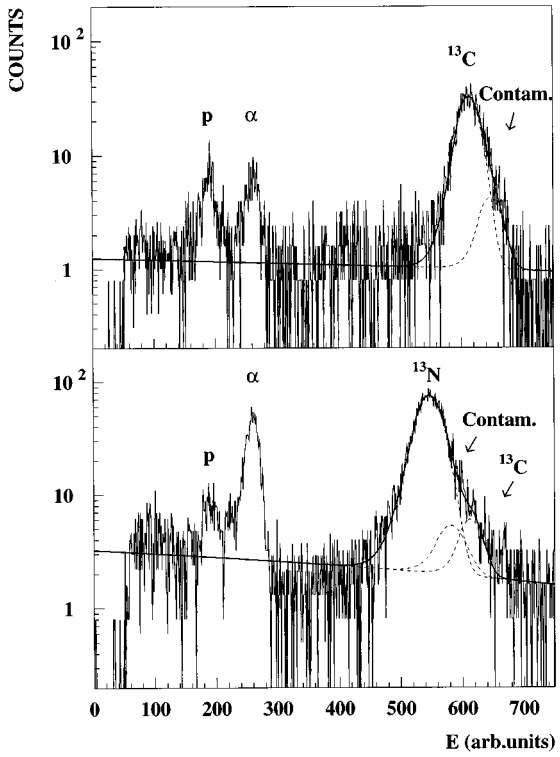

FIG. 1. Experimental spectra of $^{13}C + {}^{13}C$ (upper part) and $^{13}N + {}^{13}C$ (lower part) elastic scatterings at 10 MeV in the c.m. frame and at a mean laboratory angle of 26.75°. The energy E is in arbitrary units. The different peaks are explained in the text. The solid lines show global fits of the spectra, the dashed lines giving the contributions of each peak.

the detector energy resolution (50 keV FWHM for ^{241}Am α particles), and the energy loss and straggling in the Al degrader foil (100 keV, as estimated by GEANT [12]).

Figure 1 shows typical spectra of the $^{13}N + {}^{13}C$ (lower part) and $^{13}C + {}^{13}C$ elastic scatterings (upper part). Each peak is fitted with a Gaussian distribution matched to an exponential tail, taking into account the imperfect charge collection of the detector. These functions are superimposed on a linear background. At each angle, a global χ^2 fit is performed, using the MINUIT minimization code [13], the reliability of which was tested by simulations similar to the ones reported in Ref. [2]. Because of the weak intensity of the ^{13}C recoil peak in the $^{13}N + {}^{13}C$ spectrum, its location and shape are imposed by the main ^{13}C peak in the upper spectrum, strictly obtained at the same energy and angle, under the same conditions. The proton peak probably comes from the beam scattering on water crystals on the surface of the target, and the alpha particles are emitted by the ^{241}Am calibration source. The last contribution (''contam.'') is due to a heavy contaminant of the target. Indeed, the ^{13}C target is known to be contaminated by W or Ta coming from the filament or the crucible used to make the target. A contamination in oxygen is also observed. These contaminations are subtracted from the $^{13}N + {}^{13}C$ data in the region where the kinematical curves overlap.

A possible contamination of the ^{13}N radioactive beam by its stable isobar ^{13}C is checked on-line by scattering the beam on a Au target located 80 cm downstream the main

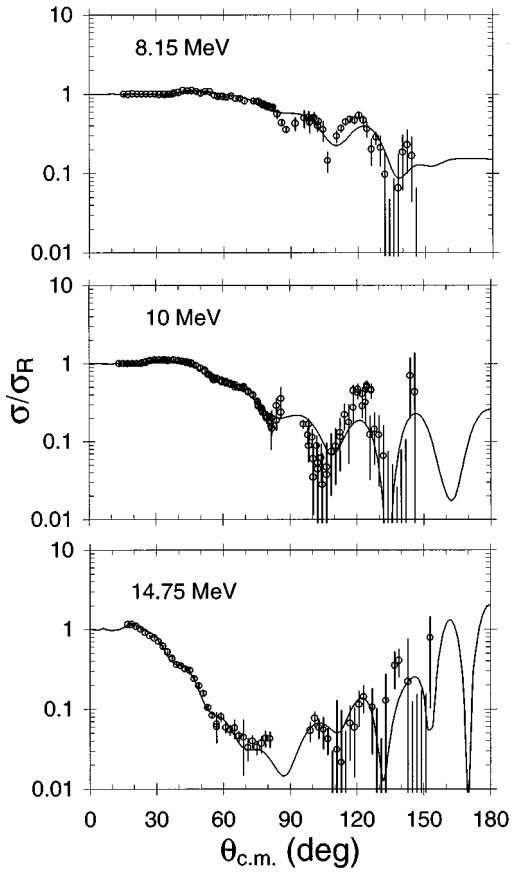

FIG. 2. Ratios of $^{13}N + {}^{13}C$ elastic cross sections to Rutherford cross sections, measured at 8.15, 10, and 14.75 MeV in the c.m. frame. Comparison with potential-model fits of the $^{13}N + {}^{13}C$ data, calculated with the potentiel (1) including the parity potential defined in Eq. (2).

^{13}C target. A silicon detector records scattered particles at 25° in the laboratory system; an Al foil in front of the detector allows a separation of ^{13}C ions from ^{13}N ions. The average ^{13}C-to-^{13}N ratio is 0.2%. The $^{13}N + {}^{13}C$ data are corrected using the corresponding $^{13}C + {}^{13}C$ data taken with the same experimental setup. The induced effect becomes really significant at large angles around 140°–150° in the c.m. frame.

The absolute cross sections are obtained by normalizing data at very small angles to the Rutherford cross sections (at 8.15 and 10 MeV) or to optical potential predictions (at 14.75 MeV), as described in [2]. The data coming from the two different detector locations are normalized to each other thanks to an imposed angular overlap. This normalization is then independent of several experimental conditions such as beam intensity and target thickness. Figure 2 shows the angular distributions of the $^{13}N + {}^{13}C$ elastic scattering, measured at 8.15, 10.0, and 14.75 MeV in the c.m. system. At the two higher energies, poor statistics prevent us from getting data around 90° c.m. No data are obtained at angles larger than 150° because of the difficulty of extracting this information. There is indeed a huge difference in intensity between the neighboring ^{13}N and ^{13}C peaks giving the cross sections at very small and very large angles, respectively. For instance, at an angle of 10° in the laboratory, the ratio of the Rutherford cross section at 20° c.m. to the Rutherford cross section at 160° c.m. is 10^3.

TABLE I. Potential parameters for the real and imaginary Woods-Saxon form factors of $V(r)$ [Eq. (1)] and for the parity term $V_p(r)$ [Eq. (2)].

V (MeV)	R (fm)	a (fm)	W (MeV)	F (MeV)	κ (fm^{-1})
−162.6	4.26	0.68	−8.8	15.2	0.45

III. POTENTIAL-MODEL ANALYSIS OF ANGULAR DISTRIBUTIONS

Different physical effects may lead to a parity dependence of the phase shifts, i.e., to a different behavior of even and odd partial waves (see Sec. IV). An odd-even variation of the phase shifts is better observed at large angles where the Coulomb contribution is minimum and interference between partial waves is large. It is usually well described in the optical model when the central nuclear potential V_N is complemented by a parity term V_p as [14–16]

$$V = V_N + (-1)^l V_p , \tag{1}$$

where l is the orbital momentum of the relative motion. The parity form factor V_p can be positive or negative, depending on the nuclei involved in the collision and on the mechanism leading to the parity dependence. Its sign determines which among the even-wave potential $V_N + V_p$ and the odd-wave potential $V_N - V_p$ is deeper. In the present section, we consider the parity potential as free from physical assumptions about its origin, and try to determine its properties with a simple form factor, without restrictions about parameter values.

The total potential V of Eq. (1) is used in an optical-model formalism to fit the data. Energy-independent Woods-Saxon form factors with the same range R and diffusivity a are chosen for the real and imaginary parts of the nuclear potential. They differ by their respective depths V and W. The choice of a common form factor is imposed by the lack of sensitivity of the fit to differences between the shapes of the real and imaginary parts. It should not be considered as physically motivated. For similar reasons, W is kept constant although one might expect an increase of this parameter with energy. The Coulomb potential is described by a sphere-sphere approximation with $r_c = 1.74$ fm [17]. As in Ref. [2], the parity potential is written as

$$V_p = F\{\exp(-\kappa r) - \exp[-(n+1)\kappa r]\}/\kappa r, \tag{2}$$

where the second exponential provides a cutoff which regularizes this parity term near the origin. As in Ref. [2], the integer value $n = 5$ is selected. Here F and κ are considered as free parameters. We discuss in the next section possible interpretations of these parameters.

The best fit that we obtain is compared with the data in Fig. 2. It corresponds to the parameters given in Table I. The potential provides an excellent fit up to about 80°. Backward structures beyond 95° are also well reproduced although the large error bars do not allow a very precise test. Data points

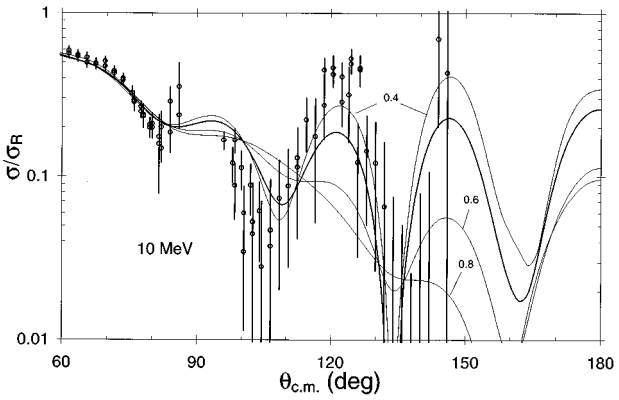

FIG. 3. Best fits of σ/σ_R at 10 MeV for different imposed κ values (see text).

are missing near 90° at the two larger energies but the results at 8.15 MeV and the existing data points at 10 and 14.75 MeV in this angular domain show that the potential is not very successful there. The cross section extrapolation towards 180° indicates that σ/σ_R might exceed unity at backward angles for $E=14.75$ MeV but not for the other two energies.

The obtained potential is deep. We did not try to establish a shallow potential as in Ref. [2]. An exact algorithm for constructing shallow from deep potentials is now available [18]. The parity term of this potential is rather similar to the parity terms obtained for ^{13}N + ^{12}C and ^{13}C + ^{12}C. Its most striking property is the low value of κ. The fitted $\kappa=0.45$ fm^{-1} is slightly smaller than the value $\kappa_n=0.47$ fm^{-1} of ^{13}C + ^{12}C, indicating a slower decrease. For ^{13}N + ^{12}C, κ_p is equal to 0.29 fm^{-1}, but this long range is weakened by a power $r^{1+\eta}$ in place of r in the denominator of the corresponding parity term V_p [2]. The additional power r^{η} is due to the Coulomb repulsion of the valence proton in ^{13}N. The parity term of ^{13}N + ^{12}C scattering can be simulated by a Yukawa term with an effective $\kappa_{\rm eff}\approx 0.36$ fm^{-1} [2], slightly smaller than the present value. Let us emphasize that larger values of κ cannot reproduce the ^{13}N + ^{13}C data, as illustrated by Fig. 3. We have fitted the cross sections at the three energies with the same central potential as in Table I but with different fixed κ values. In each case, the amplitude F was the only free parameter. The resulting amplitudes are 11.3, 26.9, and 46.8 MeV for $\kappa=0.4$, 0.6, and 0.8 fm^{-1}, respectively. In Fig. 3, one observes that $\kappa=0.6$ and 0.8 fm^{-1} are unable to reproduce the observed structure at 10 MeV. The 0.4 value is apparently satisfactory but does not provide an optimal χ^2. Allowing the central part of the potential to vary does not improve significantly the fits. Similar observations can be made at the other two energies. In particular, at 8.15 MeV, the 0.6 and 0.8 curves are essentially structureless. Finally, let us note another significant result in Table I. The sign of F is positive, which means a deeper potential for odd partial waves.

We can summarize the properties of the parity term as follows. It is unexpectedly large since its decrease is slower than for ^{13}C + ^{12}C. The sign of the parity effect is the same as for ^{13}N + ^{12}C and ^{13}C + ^{12}C. Both the range of the parity term and its sign are in contradiction with model predictions based on a simultaneous exchange of the neutron and proton valence nucleons [4]. These surprising findings point towards a mechanism for the parity effect which is different from the one anticipated. This mechanism is also not described by the model of Ref. [8]. We discuss its possible origin in the next section.

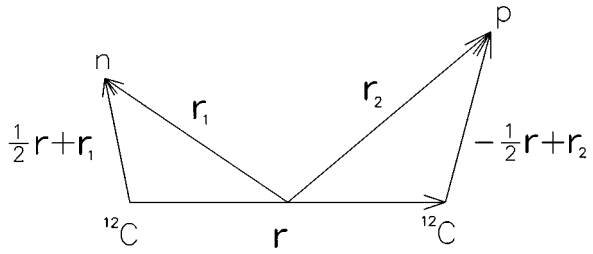

FIG. 4. Coordinate system in Eqs. (4) and (8).

IV. DISCUSSION

The parity potential can usually be explained in microscopic models [15,16] or in the nonmicroscopic molecular-orbital model [14,19,7]. In both cases, the potential is assumed to be derived from a parity projection, giving

$$V_N \pm V_p \approx \frac{\langle\phi|V|\phi\rangle \pm \langle\phi|V\Pi|\phi\rangle}{1 \pm \langle\phi|\Pi|\phi\rangle}, \tag{3}$$

where V is the sum of the different potentials acting between the nucleons of ^{13}N and the nucleons of ^{13}C, and Π is the parity operator with respect to the c.m. of the system. The wave function ϕ differs from one model to another. In microscopic models, all nucleons of the colliding nuclei are taken into account but their individual wave functions are usually described in the two-center harmonic-oscillator model. In molecular-orbital models, only valence nucleons are explicitly taken into account; other nucleons indirectly appear in phenomenological core-core and core-nucleon interactions. The wave functions of the valence nucleons can be described in a more realistic way. Here we shall make a qualitative discussion of the leading parity term at large distances. Although such a discussion does not replace more quantitative calculations, it should allow us to extract the physical origin of the observed parity effect. For simplicity, we first omit any reference to the spin quantum numbers.

Parity dependence arises from one of the matrix elements $\langle\phi|V\Pi|\phi\rangle$ or $\langle\phi|\Pi|\phi\rangle$. Usually, the typical behavior of the parity dependence can be estimated from the overlap term $\langle\phi|\Pi|\phi\rangle$. We shall evaluate its asymptotic form with a coordinate system centered at the c.m. of the ^{12}C cores (see Fig. 4). In this system, the parity operator Π simply changes the sign of all nucleon coordinates. Recoil effects are neglected. For large distances r between the ^{12}C cores, all exchanges involving the core nucleons give negligible contributions and this matrix element becomes, in all models,

$$\langle\phi|\Pi|\phi\rangle \approx \langle\varphi_n(\tfrac{1}{2}\mathbf{r}+\mathbf{r}_1)|\varphi_n(\tfrac{1}{2}\mathbf{r}-\mathbf{r}_1)\rangle \times \langle\varphi_p(-\tfrac{1}{2}\mathbf{r}+\mathbf{r}_2)|\varphi_p(-\tfrac{1}{2}\mathbf{r}-\mathbf{r}_2)\rangle, \tag{4}$$

where φ_n and φ_p are the single-particle orbitals of the valence neutron and proton, respectively. Because of the parity

operator, single-particle overlaps in Eq. (4) involve particles centered at different points. If we use the same notations as in Ref. [2], the asymptotic form is given by

$$\langle \phi|\Pi|\phi\rangle \propto \exp[-(\kappa_n+\kappa_p)r]/\kappa_n r(\kappa_p r)^{1+\eta}. \quad (5)$$

In this expression, the wave numbers are given by

$$\kappa=(2\mu E_B/\hbar^2)^{1/2}, \quad (6)$$

where E_B is the binding energy of the valence nucleon and μ is the reduced mass of the core-nucleon system. The Sommerfeld parameter of the proton reads

$$\eta=\frac{Ze^2}{\hbar(2E_B/\mu)^{1/2}}, \quad (7)$$

where Ze is the core charge. The values of κ_n, κ_p, and η have been evaluated in Ref. [2] and lead to $\kappa_n+\kappa_p=0.76$ fm^{-1} and $\eta=0.65$. The overlap term deduced from Eq. (5) decreases much too fast to explain the parity potential that fits the data. More precisely, if expression (5) is employed for V_p with an adjustable amplitude, the cross sections cannot be fitted. At 10 MeV, they are very similar to the $\kappa=0.8$ fm^{-1} curve in Fig. 3. This does not mean that this two-step mechanism, i.e., the mutual exchange of the valence proton and neutron, does not contribute to the empirical parity term that we obtain, but its effect is at best a minor contribution and is most probably negligible at the present level of accuracy of the data.

Let us now calculate the asymptotic form of the potential matrix element $\langle \phi|V\Pi|\phi\rangle$, which is dominated at large distance by components without any exchange between the ^{12}C cores,

$$\begin{aligned}\langle \phi|V\Pi|\phi\rangle \approx & \langle \varphi_n(\tfrac{1}{2}\mathbf{r}+\mathbf{r}_1)\varphi_p(-\tfrac{1}{2}\mathbf{r}+\mathbf{r}_2)|V|\varphi_n(\tfrac{1}{2}\mathbf{r}-\mathbf{r}_1)\\ & \times\varphi_p(-\tfrac{1}{2}\mathbf{r}-\mathbf{r}_2)\rangle\\ & -\langle \varphi_n(\tfrac{1}{2}\mathbf{r}+\mathbf{r}_1)\varphi_p(-\tfrac{1}{2}\mathbf{r}+\mathbf{r}_2)|V|\varphi_p(-\tfrac{1}{2}\mathbf{r}-\mathbf{r}_1)\\ & \times\varphi_n(\tfrac{1}{2}\mathbf{r}-\mathbf{r}_2)\rangle. \end{aligned} \quad (8)$$

Potential V in Eq. (8) can be separated into two parts: a term without charge exchange, to which we shall refer for simplicity as the Wigner force, and a term where the charges of the interacting nucleons are exchanged. Since orbitals depend on different coordinates, the Wigner part of the first term displays the fast decrease characteristic of products of overlaps as in Eq. (4). As a double-exchange term, the same comments as before still apply: Such an effect cannot explain the empirical parity potential. The second term vanishes for Wigner forces because of the isospin quantum numbers. However it does not vanish for charge-exchange forces. The contribution of charge exchange can be expected to decrease more slowly since it corresponds to a *single*-particle exchange, namely, of a charged pion.

Let us focus on the tail of the nucleon-nucleon interaction which is given by the one-pion exchange potential (OPEP) [20,21]

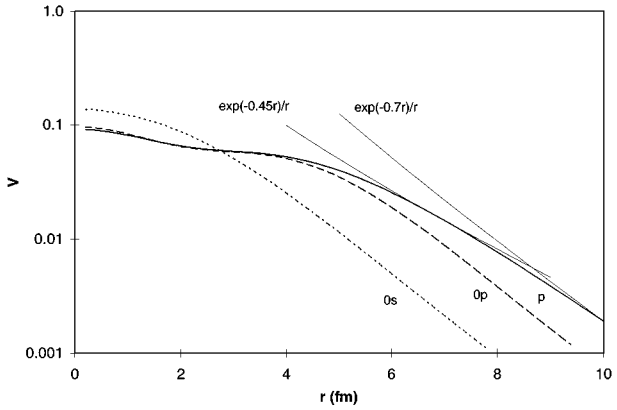

FIG. 5. Comparison of exchange matrix elements (10) for different types of orbitals with typical Yukawa terms with constants 0.7 and 0.45 fm^{-1}. The thick solid line corresponds to realistic p orbitals while the dashed and dotted lines correspond to oscillator p and s orbitals, respectively.

$$V_{\mathrm{OPEP}}=\tfrac{1}{3}f_\pi^2 m_\pi c^2(\boldsymbol{\sigma}_1\cdot\boldsymbol{\sigma}_2)(\boldsymbol{\tau}_1\cdot\boldsymbol{\tau}_2)\frac{\exp(-\kappa_\pi|\mathbf{r}_1-\mathbf{r}_2|)}{\kappa_\pi|\mathbf{r}_1-\mathbf{r}_2|}, \quad (9)$$

where $\boldsymbol{\sigma}$ and $\boldsymbol{\tau}$ represent spin and isospin Pauli matrices. In Eq. (9), m_π is the pion mass, $\kappa_\pi\approx 0.7$ fm^{-1} is the pion Compton wave number, and $f_\pi^2\approx 0.075$ is the pion-nucleon coupling constant. The charge-exchange part of Eq. (8) can be deduced from the OPEP potential by using $\boldsymbol{\tau}_1\cdot\boldsymbol{\tau}_2=2P_\tau-1$ where P_τ is the isospin exchange operator. The parity-dependent potential matrix element of Eq. (3) becomes, at large distance,

$$\begin{aligned}\langle \phi|V\Pi|\phi\rangle \approx & -\tfrac{2}{3}f_\pi^2 m_\pi c^2\langle \varphi_n(\tfrac{1}{2}\mathbf{r}+\mathbf{r}_1)\varphi_p(-\tfrac{1}{2}\mathbf{r}+\mathbf{r}_2)|\\ & \times(\boldsymbol{\sigma}_1\cdot\boldsymbol{\sigma}_2)\frac{\exp(-\kappa_\pi|\,\mathbf{r}_1-\mathbf{r}_2|)}{\kappa_\pi|\mathbf{r}_1-\mathbf{r}_2|}\\ & \times|\varphi_p(\tfrac{1}{2}\mathbf{r}+\mathbf{r}_1)\varphi_n(-\tfrac{1}{2}\mathbf{r}+\mathbf{r}_2)\rangle, \end{aligned} \quad (10)$$

where φ_n and φ_p now represent only the spatial and spin parts of the wave functions, without the isospin components. We have used the fact that φ_n and φ_p have the same parity. The important point in Eq. (10) is that individual functions depending on the same variable are now centered around the same point. For r tending to infinity, the asymptotic form of Eq. (10) is shown in the Appendix to be

$$\langle \phi|V\Pi|\phi\rangle \propto \exp(-\kappa_\pi r)/\kappa_\pi r. \quad (11)$$

We observe that the decrease of this expression is also too fast to explain the parity term (2). However, this asymptotic behavior is reached at large distances only. We now argue that a slower decrease occurs at intermediate distances, which looks similar to the decrease of the empirical parity potential.

This is illustrated by Fig. 5 where the matrix element (10) is calculated under different assumptions and compared with exponential decreases proportional to $\exp(-\kappa_\pi r)/r$ and to $\exp(-\kappa r)/r$ with $\kappa=0.45$ fm^{-1} as given in Table I. Normalizations should not be considered in the comparison. The matrix element is calculated under three different assumptions: with $0s$ and $0p$ oscillator orbitals, and with realistic

p orbitals. The $0s$ case (dotted line) is not physically useful but can easily be checked by the reader with the help of Eq. (A4) of the Appendix. One observes that the asymptotic behavior (11) is only reached beyond 5 fm for these $0s$ orbitals. With $0p$ oscillator orbitals, a longer analytic expression leads to the dashed line which becomes asymptotic near 6.5 fm. Between 4 and 7 fm, the average decrease is however slower than for $0s$ orbitals. Realistic individual wave functions for the p orbitals are obtained by solving Schrödinger equations with the same $n+{}^{12}\mathrm{C}$ and $p+{}^{12}\mathrm{C}$ potentials as in Ref. [2]. The matrix element (solid line) then tends more slowly towards its asymptotic form which is only reached beyond 9 fm (the Yukawa function with $\kappa_\pi \approx 0.7$ fm^{-1} is normalized to the matrix element at 10 fm). Before reaching that asymptotic regime, the decrease of the matrix element is quite slow. One understands that it can be simulated with a Yukawa form factor with κ smaller than κ_π (the Yukawa function with $\kappa = 0.45$ fm^{-1} is normalized to the matrix element at 6.8 fm). At a qualitative level, the slow decrease of the parity potential is therefore not surprising when charge-exchange forces are taken into account.

Let us now discuss qualitatively the sign of the parity term of the potential. Because we are concerned with $p1/2$ orbitals, the treatment of the spin parts requires angular momentum recouplings which are beyond the scope of the present work. Let us simplify the discussion by using an approximation where the nucleon spin is decoupled from the orbital momentum as in s orbitals. For spin-1/2 nuclei, the differential cross section reads

$$\frac{d\sigma}{d\Omega} = \frac{1}{4}|f_0|^2 + \frac{3}{4}|f_1|^2, \tag{12}$$

where f_0 and f_1 correspond to the channel spins $S=0$ and $S=1$, respectively. In Sec. III, we have approximated this expression with a single average amplitude f since the potential is spin independent. In fact the two amplitudes, when treated separately, may require different parity potentials and this complicates the sign determination. However, if we take into account the fact that ^{13}N and ^{13}C belong to a same isospin multiplet, the different partial waves must satisfy

$$(-1)^{l+S+T} = -1. \tag{13}$$

Hence, by calculating mean values of $(\boldsymbol{\sigma}_1 \cdot \boldsymbol{\sigma}_2)(\boldsymbol{\tau}_1 \cdot \boldsymbol{\tau}_2)$, one readily obtains that the odd-l potential is deeper at large distances than the even-l one in the second term of Eq. (8) for both spin values. This agrees with the positive value of the constant F found in Sec. III. Moreover, if angular momentum recouplings do not complicate the situation too much, one might expect the same behavior in other collisions between mirror heavy ions, i.e., a similar slow exponential decrease and the same sign, since the present discussion mostly relies on the asymptotic form of the nucleon-nucleon interaction.

The present discussion will have to be verified by more elaborate calculations. Such a calculation has already been performed in Ref. [8]. However, the conclusions of that work neither confirm nor contradict the present analysis because the authors have used a pure Wigner force. The second term of our Eq. (8) vanishes in that case and long-range parity effects are not found. Their parity dependence resembles the one deduced from Eq. (5) and the resulting cross sections are similar to the $\kappa = 0.8$ fm^{-1} curve of Fig. 3.

V. CONCLUSION

We have measured the ^{13}N + ^{13}C elastic scattering at three energies from just above to about twice the Coulomb barrier. The data display a significant rise at large angles. A central optical potential accurately fits the cross sections up to about 80°. The behavior at large angles is well fitted with the introduction of a slowly decreasing parity term. In fact, contrary to predictions [4,8], the present parity effect is large, and is of a comparable magnitude with the effects encountered in the ^{13}C + ^{12}C and ^{13}N + ^{12}C scatterings [14,2].

In spite of rather large error bars at backward angles, the fact that a consistently good fit is obtained at three different energies shows that the optical potential is fairly well established. Its long range is incompatible with mechanisms involving more than a single exchange because they imply a product of at least two overlap matrix elements and lead to a faster decrease. The decrease is even slower than the asymptoptic form of a one-pion exchange matrix element, which is related to the pion Compton wave number. However, it is compatible with matrix elements taking the spatial extension of individual wave functions into account. At distances between 5 and 8 fm, the matrix element indeed decreases more slowly than its asymptotic form. The sign of the parity effect is also, with some simplifying assumptions, explained with simple physical arguments.

The present optical-model results encourage the use of more elaborate molecular-orbitals models in order to describe the ^{13}N + ^{13}C elastic scattering. However, these calculations should generalize the assumptions of Ref. [8] and take an explicit account of charge-exchange contributions to the nuclear forces. Such models are necessary to establish the validity of the qualitative arguments that we propose in Sec. IV. They may, however, have to take into account the important ^{14}N + ^{12}C and ^{14}N + ^{12}C* channels which must dominate the absorption at these low energies. Microscopic models [15,16] can also address the same problem but with other effective forces than usually assumed, i.e., with forces reproducing the OPEP behavior at large distances.

The existence of a strong exchange effect in ^{13}N + ^{13}C scattering calls for an experimental confirmation. Further data about this system would be useful when better statistics and larger scattering angles will become reachable. Also data points around 90° would be useful for a more accurate determination of the ^{13}N + ^{13}C interaction. Information from other collisions between mirror nuclei would also provide a confirmation of the exchange mechanism. Among candidates for radioactive-beam experiments which might become feasible in a not-too-distant future are ^{15}O + ^{15}N with spin 1/2 nuclei or ^{11}C + ^{11}B and ^{17}F + ^{17}O with higher spins. In principle the importance and sign of the parity effect should be quite similar to the ^{13}N + ^{13}C case in all these systems if the mechanism that we suggest here is valid.

ACKNOWLEDGMENTS

We acknowledge the support of the cyclotron staff, the help of P. Collin and P. Demaret (Louvain-la-Neuve) and of

M. Schmitt (Erlangen) for preparing the targets, and of H. Murakami (Rikkyo) for preparing the detector electronics. Four of us (P. Descouvement, P. Lipnik, J.-M. Sparenberg, and J. Vanhorenbeeck) acknowledge the support of the National Fund for Scientific Research, Belgium. This text presents research results of the Belgian program on interuniversity attraction poles initiated by the Belgian Federal Services for Scientific, Technical, and Cultural Affairs. Some travel expenses are supported in part by the Joint Research of Monbusho International Scientific Research Program under Program No. 06044205.

APPENDIX

First we calculate the matrix element in (10) for $0s$ oscillator basis functions with a common oscillator parameter b. To this end, we employ the integral representation [22]

$$\frac{\exp(-\kappa r)}{r}=\frac{2}{\sqrt{\pi}}\int_0^\infty \exp\left(-\frac{\kappa^2}{4t^2}-t^2r^2\right)dt. \tag{A1}$$

With Gaussian wave functions centered at $-r/2$ and $r/2$ along the z axis, one is led to calculate the simple expression

$$\begin{aligned}&\langle\varphi(\tfrac{1}{2}\mathbf{r}+\mathbf{r}_1)\varphi(-\tfrac{1}{2}\mathbf{r}+\mathbf{r}_2)|\exp[-t^2(\mathbf{r}_1-\mathbf{r}_2)^2]\\&\quad\times|\varphi(\tfrac{1}{2}\mathbf{r}+\mathbf{r}_1)\varphi(-\tfrac{1}{2}\mathbf{r}+\mathbf{r}_2)\rangle\\&=(1+2b^2t^2)^{-3/2}\exp[-t^2r^2/(1+2b^2t^2)].\end{aligned} \tag{A2}$$

With the change of variable,

$$u=\sqrt{2}bt/(1+2b^2t^2)^{1/2}, \tag{A3}$$

the spatial part of the matrix element in Eq. (10) becomes

$$\begin{aligned}&\left\langle\varphi(\tfrac{1}{2}\mathbf{r}+\mathbf{r}_1)\varphi(-\tfrac{1}{2}\mathbf{r}+\mathbf{r}_2)\right|\frac{\exp(-\kappa|\mathbf{r}_1-\mathbf{r}_2|)}{|\mathbf{r}_1-\mathbf{r}_2|}\\&\quad\times\left|\varphi(\tfrac{1}{2}\mathbf{r}+\mathbf{r}_1)\varphi(-\tfrac{1}{2}\mathbf{r}+\mathbf{r}_2)\right\rangle\\&=\left(\frac{2}{\pi b^2}\right)^{1/2}\exp\left(\frac{b^2\kappa^2}{2}\right)\\&\quad\times\int_0^1\exp\left(-\frac{r^2u^2}{2b^2}-\frac{b^2\kappa^2}{2u^2}\right)du.\end{aligned} \tag{A4}$$

For r large, the exponential in the integral becomes small for $u\approx 1$ and the upper limit 1 can be to a good approximation replaced by ∞. Then with Eq. (A1), one recovers the asymptotic behavior (11).

The result (A4) can easily be extended to p orbitals and to oscillator states with different oscillator parameters. The final expressions are significantly longer and we do not display them here. These analytic expressions are also useful for a calculation involving realistic (nonoscillator) p orbitals. In a first step, the neutron and proton orbitals are calculated numerically with the potentials described in Ref. [2]. They are then expanded on a basis of oscillator $0p$ states with different oscillator parameters, the linear coefficients being determined with a least-squares fit. Good results are already obtained with ten basis functions. The matrix element displayed in Fig. 5 is finally obtained by a combination of matrix elements such as Eq. (A4) extended to $0p$ states with different oscillator parameters.

[1] *Proceedings of the Second International Conference on Radioactive Nuclear Beams*, Louvain-la-Neuve, 1991, edited by Th. Delbar (Adam Hilger, Bristol, 1992); *Proceedings of the Third International Conference on Radioactive Nuclear Beams*, East Lansing editions, 1993, edited by D.J. Morrissey (Frontières, Gif-sur-Yvette, 1993).

[2] E. Liénard, D. Baye, Th. Delbar, P. Descouvemont, P. Duhamel, W. Galster, M. Kurokawa, P. Leleux, I. Licot, P. Lipnik, C. Michotte, T. Motobayashi, A. Ninane, J. Vanhorenbeeck, and J. Vervier, Phys. Rev. C **52**, 775 (1995).

[3] E. Liénard, D. Baye, Th. Delbar, P. Descouvemont, P. Duhamel, W. Galster, M. Kurokawa. P. Leleux, I. Licot, P. Lipnik, C. Michotte, T. Motobayashi, A. Ninane, J. Vanhorenbeeck, and J. Vervier, in *Proceedings of the International Conference on Nucleus-Nucleus Collisions*, Taormina, 1994 [Nucl. Phys. **A583**, 783 (1995)].

[4] D. Baye, Th. Delbar, P. Descouvemont, P. Duhamel, W. Galster, P. Leleux, E. Liénard, P. Lipnik, C. Michotte, J. Vanhorenbeeck, and J. Vervier, in *Proceedings of the Second International Conference on Radioactive Nuclear Beams*, Louvain-la-Neuve, 1991, edited by Th. Delbar (Adam Hilger, Bristol, 1992), p. 173.

[5] M. Ivanovich, P.G. Young, and G.G. Ohlsen, Nucl. Phys. **A110**, 441 (1968); A.D. Bacher, R.J. Spiger, and T.A. Tombrello, *ibid.* **A119**, 481 (1968); R. Vlastou, J.B.A. England, O. Karban, and S. Baird, *ibid.* **A292**, 29 (1977).

[6] R.N. Boyd, M.S. Islam, G. Kolnicki, M. Farrell, T.F. Wang, K.E. Sale, and G.J. Mathews, in *Proceedings of the First International Conference on Radioactive Nuclear Beams*, Berkeley, 1989, edited by W.D. Myers, J.M. Nitschke, and E.B. Norman (World Scientific, Singapore, 1990), p. 311.

[7] M.A. Nagarajan and J.P. Vary, Phys. Rev. C **43**, 281 (1991).

[8] A.T. Kruppa, M.A. Nagarajan, and J.P. Vary, Phys. Rev. C **47**, R451 (1993).

[9] M. Steiner, S.M. Austin, D. Bazin, W. Benenson, C.A. Bertulani, J.A. Brown, M. Fauerbach, M. Hellström, E. Kashy, J.H. Kelley, R.A. Kryger, T. Kubo, N.A. Orr, R. Pfaff, B.M. Sherrill, M. Thoennessen, S.J. Yennello, B.M. Young, and P.D. Zecher, Phys. Rev. Lett. **76**, 26 (1996).

[10] P. Van Duppen, P. Decrock, M. Huyse, Th. Delbar, W. Galster, P. Leleux, I. Licot, E. Liénard, P. Lipnik, M. Loiselet, C. Michotte, G. Ryckewaert, J. Vervier, P. Duhamel, and J. Vanhorenbeeck, Nucl. Instrum. Methods B **70**, 393 (1992); Nucl. Phys. **A553**, 837c (1993).

[11] S. Trentalange, S.-C. Wu, J.L. Osborne, and C.A. Barnes, Nucl. Phys. **A483**, 406 (1988).

[12] R. Brun, CERN report, 1994.

[13] F. James and M. Ross, CERN Report No. D506, 1983.

[14] W. von Oertzen and H.G. Bohlen, Phys. Rep. **19C**, 1 (1975).
[15] D. Baye, J. Deenen, and Y. Salmon, Nucl. Phys. **A289**, 511 (1977).
[16] D. Baye, Nucl. Phys. **A460**, 581 (1986).
[17] D. Baye, Nucl. Phys. **A272**, 445 (1976).
[18] D. Baye, G. Lévai, and J.-M. Sparenberg, Nucl. Phys. **A599**, 435 (1996).
[19] B. Imanishi and W. von Oertzen, Phys. Rep. **155**, 29 (1987).
[20] J.M. Eisenberg and W. Greiner, *Microscopic Theory of the Nucleus*, *Nuclear Theory*, Vol. 3 (North-Holland, Amsterdam, 1972).
[21] V.G.J. Stoks, R.A.M. Klomp, C.P.F. Terheggen, and J.J. de Swart, Phys. Rev. C **49**, 2950 (1994).
[22] S. Okabe, Prog. Theor. Phys. **68**, 1790 (1982).